tvst

Cornea & External Disease

Regional Biomechanical Weakening in Keratoconus Corneas Detected by In Vivo High-Frequency Ultrasound Elastography

Sunny Kwok[1], Xueliang Pan[2], Manqi Pan[1], Zihao Chen[1], Madison Ammon[3], Andrew Hendershot[4], and Jun Liu[1,3,4]

[1] Department of Biomedical Engineering, The Ohio State University, Columbus, OH, USA
[2] Department of Biomedical Informatics, The Ohio State University, Columbus, OH, USA
[3] Biophysics Graduate Program, The Ohio State University, Columbus, OH, USA
[4] Department of Ophthalmology and Visual Sciences, The Ohio State University, Columbus, OH, USA

Correspondence: Jun Liu, Department of Biomedical Engineering, The Ohio State University, 140 W. 19th Ave, Columbus, OH 43210, USA. e-mail: liu.314@osu.edu

Received: August 27, 2024
Accepted: February 25, 2025
Published: March 26, 2025

Keywords: ultrasound elastography; corneal biomechanics; ocular pulse; high frequency ultrasound; keratoconus

Citation: Kwok S, Pan X, Pan M, Chen Z, Ammon M, Hendershot A, Liu J. Regional biomechanical weakening in keratoconus corneas detected by in vivo high-frequency ultrasound elastography. Transl Vis Sci Technol. 2025;14(3):22, https://doi.org/10.1167/tvst.14.3.22

Purpose: In vivo biomechanical characterization of the cornea remains a challenge. We have developed a high-resolution ultrasound elastography technique, termed ocular pulse elastography (OPE), to measure corneal deformation in response to the intraocular pressure (IOP) pulsation at each heartbeat. In this study, we aimed to compare corneal axial strains (CASs) between patients with keratoconus and normal subjects and evaluate the spatial mapping of CAS in high grade keratoconus.

Methods: Forty patients with keratoconus (63 eyes) and 40 normal controls (80 eyes) were enrolled in this study. Each eye underwent 4 ultrasound measurements using the Vevo2100 high-frequency ultrasound system. Each measurement acquired 1000 continuous B-mode scans in 8 seconds. Corneal axial displacements and strains were quantified using an ultrasound speckle tracking algorithm.

Results: CAS magnitude was significantly higher in keratoconus than normal corneas ($-0.13\% \pm 0.09\%$ vs. $-0.06\% \pm 0.04\%$, $P < 0.001$) with an increasing trend in higher grades ($P < 0.001$). CAS in keratoconus corneas had a greater spatial variance as higher strains were observed in the cone center than its surrounding regions in grade 3 and 4 keratoconus corneas.

Conclusions: Our results showed that high-frequency ultrasound elastography was able to detect and quantify the larger deformation of keratoconus corneas than normal corneas in response to the natural fluctuations of IOP at each heartbeat, and it also detected the spatial variance showing greater deformation in the cone region.

Translational Relevance: High-resolution ultrasound may provide a sensitive tool for quick, spatially resolved characterization of corneal biomechanics to aid keratoconus detection and diagnosis.

Introduction

Corneal shape is critical for visual acuity. In keratoconus, a region of the cornea forms a conical protrusion with local steepening and thinning. This distorted shape leads to vision impairment. Current clinical diagnosis is primarily based on detecting corneal shape change using topography and tomography; however, these methods have difficulty differentiating subtle changes, such as those in subclinical keratoconus.

Microstructural and compositional changes are also observed in the keratoconic cornea. These changes include loss of keratocytes, reduced crosslinks, and disorganized collagen network in the cone region.[1–4] Linked to these changes are changes in corneal biomechanical properties. Mechanical testing on corneal strips revealed a reduced tensile modulus in keratoconus corneas.[5,6] The Ocular Response

Analyzer (ORA; Reichert Instruments, Depew, NY, USA) and the Scheimpflug-based Corvis ST (Oculus, Wetzlar, Germany) showed greater deformation and less resistance to air puff in keratoconus corneas.[7–9] These global measurements point to an overall mechanical weakening, but do not quantify localized biomechanical changes which are believed to be the primary cause of disease onset and an indicator of progression.[10,11] Imaging-based methods are thus developed to resolve and more sensitively detect and quantify localized biomechanical changes.[12–15]

Our laboratory has developed a high-frequency ultrasound elastography method, called the ocular pulse elastography (OPE), to provide in vivo characterization and spatial mapping of the human cornea's biomechanical response to the ocular pulse.[15–17] During each ultrasound measurement, an 8-second video of one corneal cross-section is acquired to quantify its cyclic deformation over 8 to 12 heartbeats. We analyzed the radiofrequency (RF) data instead of the images to achieve accurate and sensitive detection of small displacements and strains associated with the ocular pulse.[15,16] Our method overcomes involuntary eye motion to successfully track the cornea's response to the ocular pulsation, and demonstrated excellent in vivo repeatability in measuring the human cornea despite noticeable eye drifts and saccades.[17]

Using this method, we detected a significantly larger cyclic corneal axial displacement (CAD) in patients with keratoconus.[18] We also showed that CAD increased further at higher grades. These results confirmed the expected overall biomechanical weakening of keratoconus corneas, but localized changes were not evaluated in that study. Our previous studies indicated that CAD itself was not a sensitive parameter to evaluate the spatial variations of biomechanical responses, and it could potentially be affected by whole eye axial motion. The goal of the current study was to quantify and analyze corneal axial strain (CAS), a step further to compute the spatial gradients of CAD in the axial direction; and to evaluate whether biomechanical weakening, as indicated by a larger CAS, is more pronounced in the cone region of the keratoconic cornea. Quantification of small strains associated with the ocular pulse is challenging because strain is the spatial gradient of displacements (mathematically a derivative process) and more susceptible to noise. In this study, we developed a strategy taking advantage of the multiple cardiac cycles in each measurement and multiple measurements in each eye to robustly characterize CAS. In addition, we analyzed the regional responses and compared the cone center and its surrounding regions in high-grade keratoconus to evaluate the spatial variations of the mechanical weakening.

Materials and Methods

Participants

Written informed consent was obtained from all participants after explanation of the nature and possible consequences of the study, in adherence to the tenets of the Declaration of Helsinki and with approval of the Ohio State University Institutional Review Board. Forty normal volunteers with no known corneal pathology/surgeries or clinical signs of keratoconus were enrolled in this study. Forty patients with a clinical diagnosis of keratoconus were recruited from those receiving eye care at the Ohio State University Havener Eye Institute. Keratoconus was identified by characteristic refractive and slit-lamp signs that include unstable refraction, oblique astigmatism, irregular retinoscopic and keratometry mires, and biomicroscopic signs such as Vogt striae, Fleischer ring, etc., and no history of corneal surgery in at least one eye. Eyes undergoing crosslinking treatment or with pellucid marginal degeneration, corneal scarring, or other pathology, were excluded from the study.

Measurement Setup and Testing Protocols

Each subject underwent topography, tomography, intraocular pressure (IOP), and ultrasound OPE measurements during one visit. First, corneal topography and tomography were acquired using Pentacam (Oculus, Wetzlar, Germany). Corneal curvature map, thickness map, K_{max}, and thinnest pachymetry were recorded. Three repeated measurements were obtained in each eye. Topography and tomography of keratoconus eyes were reviewed by a corneal specialist (author AH) to determine the keratoconus grade (0 to 4 from mild to severe) using the Belin ABCD grading system.[17,19] The system stages keratoconus using four key parameters: (1) A = anterior corneal curvature, (2) B = posterior corneal curvature, (3) C = corneal thickness at the thinnest point), and (4) D = distant visual acuity, allowing for a more comprehensive assessment of the disease. Subclinical keratoconus in the contralateral eye of patients diagnosed with keratoconus was assigned to grade 0. Second, three repeated measurements of diastolic IOP and ocular pulse amplitude (OPA) were obtained in each eye using a PASCAL Dynamic Contour Tonometer (DCT; Ziemer USA, Alton, IL, USA). Third, each eye was measured

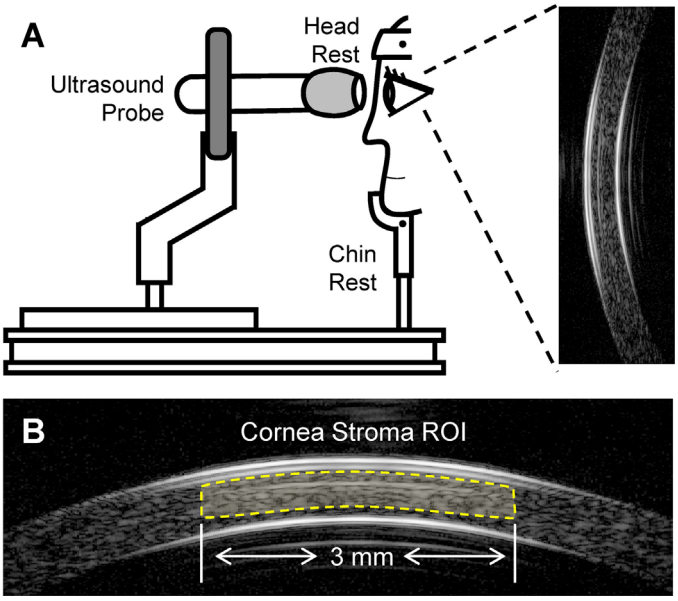

Figure 1. (**A**) The subject is stabilized for the OPE measurement with the head secured to a chin-and-head rest mounted on an antivibration table. One thousand frames of ultrasound B-mode images and RF data of the cornea centered at the apex are collected over a period of 8 seconds. (**B**) The central 3-mm corneal stroma is automatically segmented out as the region of interest (ROI) for OPE analysis.

with a high-frequency ultrasound imaging system using a 50 MHz probe (MS700, Vevo 2100; FujiFilm VisualSonics, Inc., Toronto, Canada). The ultrasound system has a digital RF mode that enables access to and saving of RF data. Four repeated ultrasound measurements were recorded in each eye to obtain CAD and CAS. Details of the ultrasound measurements are described previously[17,18] and summarized below.

The subject sat with their head placed on a head-and-chin rest mounted on an anti-vibration table (ScienceDesk Workstations; Thorlabs, Newton, NJ). The ultrasound probe was secured to a holder mounted on a slit lamp (Fig. 1A). The probe surface was covered with a cellulose membrane which enclosed a layer of alginate gel as a standoff. The outer surface of the cellulose membrane was covered by a layer of eye lubricating gel (GenTeal Severe Dry Eye Relief; Alcon, Inc., Ft. Worth, TX, USA). Anesthetic eye drops (Tetracaine HCl 0.5%; Bausch & Lomb, Bridgewater, NJ, USA) were applied to both eyes prior to measurements.

For each measurement, the subjects were asked to keep their eyes open and hold their gaze on a distance target for up to 15 seconds. During this time, the ultrasound probe was advanced toward the eye until the GenTeal gel on the probe surface established contact with the cornea. The corneal image on the monitor screen provided guidance for the operator to position the probe to the cornea apex (see Fig. 1A). One thousand consecutive B-mode frames and its RF data of the central 5.7 mm of the cornea were then acquired for 8 seconds at 128 frames per second along the nasal-temporal meridian. Four repeated measurements were obtained in each eye, with additional gel applied to the probe surface as needed. The right eye (OD) was measured first, followed by the left eye (OS) in all subjects.

Corneal Displacements Calculated From Ultrasound Speckle Tracking

Corneal displacements were calculated using an ultrasound speckle tracking algorithm described previously.[20–22] Briefly, the RF data were acquired and stored as 300 A-lines spaced at 19 μm lateral intervals and sampled at approximately 1.5 μm axial intervals. To perform speckle tracking on RF data, a region of interest (ROI) was defined in the reference frame (i.e. first acquired frame) by automatic segmentation to generate an ROI approximately 3 mm in width within the corneal stroma that contains high acoustic signals for optimal speckle tracking (Fig. 1B).[17] A dense rectangular grid was defined within the ROI, with about 200 grid points spaced by 13 × 10 pixels (axial × lateral), or approximately 19.5 μm × 190 μm. Kernels containing 51 × 41 pixels each were centered at each grid point with a 75% overlap.[15,16] To compute the displacement at each grid point, the unique speckle pattern within the kernel centered at the grid point was tracked in subsequent frames using cross-correlation. A maximum correlation coefficient was considered as the best match, and the corresponding kernel center was designated as the new location of the displaced grid point. Spline interpolation was used for subpixel tracking. The accuracy of the ultrasound elastographic technique for displacement and strain measurements has been validated and reported in our previous publications.[15,20,21,23] Using simulated RF data, we showed accurate detection of strains down to 0.01% axially and 0.025% laterally (percent error $< 10\%$).[15] Our previous in vivo studies also showed that high-quality ultrasound speckle tracking was successful despite normal involuntary eye movements, such as drifts or microsaccades. The high frame rate and adequate imaging plane thickness made it possible to track and analyze ocular pulse related corneal axial displacements in most subjects.[17,18,24]

To reduce processing time and improve tracking accuracy, we down-sampled the 1000 scanned frames by a factor of 5 and calculated displacements between

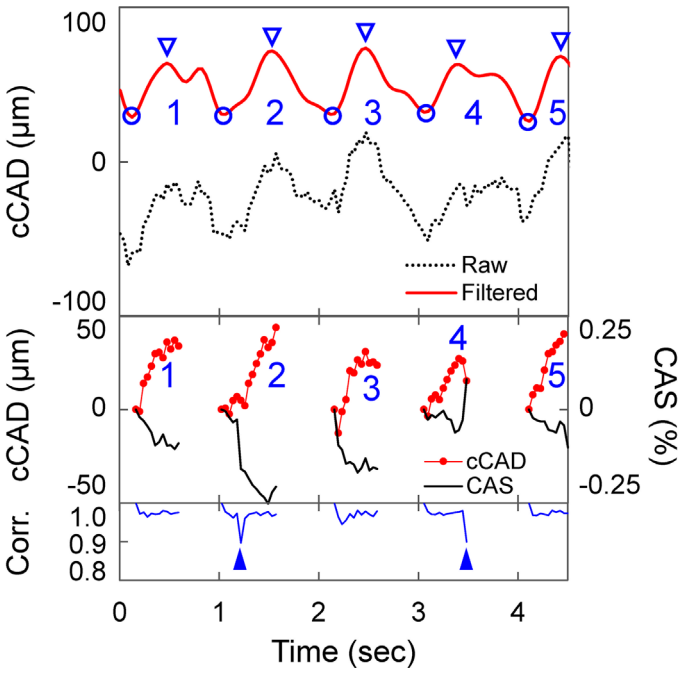

Figure 2. Raw (*dotted line*) and bandpass filtered (*red solid line*) cumulative corneal displacement (cCAD) curves from a representative normal eye show that bandpass filtering was effective for identification of cardiac cycles and their respective trough (*blue circle*) and peak (*blue triangle*) frames. Corneal axial strain (CAS) was calculated for consecutive frames between trough and peak for each cycle. Cycles with any stepwise correlation coefficient lower than 0.9 (*arrowhead*) were removed from analysis.

200 down-sampled frames. The displacement vector of each grid point was obtained between 2 consecutively sampled frames and accumulated over all 200 frames. Because the accuracy of axial displacement was much higher than that of lateral displacement due to higher spatial resolution and sampling density in the axial direction,[15] only axial displacements were used for further analysis in this study. The average axial displacement of all grid points within the ROI was plotted as the cumulative corneal axial displacement (cCAD; Fig. 2).

The cCAD signal was bandpass filtered to remove noise to better identify trough and peak frames as described in our previous work.[18] Briefly, the heart rate frequency (F_{HR}) for each measurement was first identified automatically from the frequency spectrum. Frequency components below 0.9 F_{HR}, above 3 F_{HR}, and those with magnitudes below 10% of the maximum peak were removed. Cardiac cycles were then identified from the filtered curve by their trough and peak frames (see Fig. 2). Troughs were first identified as local minima, and the corresponding peak was identified as the maxima between two consecutive troughs no less than one-fifth of the average heart rate period from the first trough. Cardiac cycles with correlation coefficients below 0.9 were considered as unsatisfactory tracking and removed from further analysis.

Corneal Strain Calculation Using Robust Linear Regression Estimation

For each identified cycle, corneal displacements were recalculated using the same method as above but taking the trough frame as the starting reference frame and ending three frames after the identified peak (see Fig. 2). This ensures that the calculated strains were from the trough to peak. The CAS was calculated as the axial gradient of the axial displacement using *robustfit*, a MatLab function for robust linear regression estimation (The Math Works, Inc., version 2020a). The CAS values from cycles in the same measurement were averaged as the CAS value for that measurement of the eye. Combining the CAS values from all 4 measurements in each subject, outliers were defined as values less or greater than 1.5 times of interquartile range of the first and third quartiles and removed. The remaining CAS was averaged to yield a single value for each eye. All strain analysis used directly calculated strain values at the kernel level. For visualization, strain maps were generated by interpolating CAS to the pixel level using bilinear interpolation.

Regional Segmentation and Analysis of Keratoconus Cone

In patients with keratoconus of high grades (grade 3 and 4) where local thinning was more apparent in the ultrasound images, we performed an analysis between the cone center and the surrounding regions. The following definitions of cone center and surrounding regions are used in the present study. The cone center is defined as the 500 μm width of corneal stroma centered around the thinnest point as identified from the ultrasound B-mode image. The rest of the cornea within the ROI (as defined in Fig. 1B) was considered as the surrounding region. The strain data in both regions were analyzed for comparison. It is noted that the definition of the cone center we used was based on the cross-sectional ultrasound images, which may or may not fully capture the clinical cone center identified from topography. We chose this definition to compare the regional differences assuming the thinnest region in the ultrasound image is at least closer to the cone, if not the true cone, than the other regions in the scanned cross-section.

Statistical Analysis

The primary objective of this study was to evaluate CAS in normal and keratoconus eyes, and to test if they were significantly different between the two groups. A sample size of 40 subjects (up to 80 eyes) per group provided at least 90% power to detect an effect size of 0.75 (Cohen's d = 0.75) between normal and keratoconus eyes. The effect size of 0.75 was chosen based on the modulus difference between these two groups reported by Andreassen et al.[5] Considering the moderate association between the paired eyes from the same individual, the actual power could be higher.

Summary statistics (mean and standard deviations) were generated for age, IOP, OPA, K_{max}, thinnest pachymetry and CAS in normal and keratoconus eyes. To compare between groups, linear mixed models for repeated measures were used to account for the association between paired eyes of the same subject where group was the fixed effect and subject was the random effect. Sensitivity analysis after adjusting for age, IOP, and OPA as covariates were also conducted to confirm if the conclusions of the differences were robust to model selection. Pearson correlations were used to summarize the associations of the measures between OD and OS by different groups. Association of CAS and keratoconus grade were also evaluated using linear mixed models for repeated measures where grade (keratoconus grade ranged from 0 to 4 and the normal grade was assigned as −1) was set as fixed effect and subject as random effect. Comparisons between keratoconus cone and surrounding regions were evaluated using the paired *t*-test. The associations among CAS and age, IOP, OPA, K_{max}, and thinnest pachymetry were also explored using scatter plots. All statistical analyses were conducted using SAS (version 9.4; SAS Institute Inc., Cary, NC, USA). A P value $\leq$ 0.05 is considered as statistically significant.

Results

Eighty eyes from 40 normal subjects and 63 eyes from 40 patients with keratoconus were included in this study. Pentacam readings confirmed the absence of abnormal topography in normal subjects. Seventeen eyes from patients with keratoconus were excluded based on our exclusion criteria, such as corneal scarring. Ultrasound B-mode images, and Pentacam thickness and curvature maps from representative normal subjects and patients with keratoconus are shown in Fig. 3. Pentacam, DCT, and OPE measurements, and comparisons between normal and keratoconus groups are summarized in the Table.

Thinnest pachymetry and K_{max} were significantly different between normal and keratoconus corneas ($P < 0.001$; see the Table). CAS magnitude was significantly higher in patients with keratoconus than the normal subjects (−0.13 ± 0.09% vs. −0.06 ± 0.04%, $P < 0.001$; see the Table). Age, IOP, and OPA were significantly different between the two groups, and sensitivity analysis considering age and IOP as covariates yielded the same conclusions with slightly changed P values (see the Table).

Representative CAS spatial maps for a normal subject and a patient with keratoconus at each grade are presented in Fig. 4. Grading according to the Belin ABCD system identified 6 eyes in grade 0, 7 in grade 1, 16 in grade 2, 17 in grade 3, and 17 in grade 4. The mean CAS for each grade was −0.12 ± 0.06%, −0.06 ± 0.03%, −0.12 ± 0.09%, −0.10 ± 0.07%, and −0.20 ± 0.11%, respectively. Mean CAS magnitude was found to significantly increase with higher keratoconus grade ($P < 0.001$; Fig. 5).

We further plotted the CAS profile over the width of the keratoconus cornea, which again showed a higher magnitude around the cone center (Fig. 6). The CAS in the cone center and surrounding regions of grade 3 and 4 keratoconus eyes ($n = 34$ eyes) were compared, showing a significantly higher CAS in the cone center than the surrounding region (−0.23 ± 0.13% vs. −0.14 ± 0.10%, $P < 0.001$; Fig. 7). Both the cone center and surrounding regions in grades 3 and 4 keratoconus eyes had significantly higher CAS compared with normal corneas ($P < 0.001$ and $P = 0.002$, respectively; see Fig. 7).

Combining the normal and keratoconus data points, CAS was significantly correlated between the left and right eyes (R = 0.63, $P < 0.001$; Fig. 8) in the same subject, indicating a level of bilateral symmetry. When the normal and the keratoconus groups were examined separately, the bilateral symmetry was weaker but remained statistically significant (normal: R = 0.38, $P = 0.016$ and keratoconus: R = 0.61, $P = 0.002$).

In the normal group, CAS was not correlated with age, heart rate, IOP, OPA, K_{max}, or thinnest pachymetry. In the keratoconus group, CAS was not correlated with age, heart rate, IOP, or OPA, but was significantly correlated with K_{max} and pachymetry (R = −0.48, $P < 0.001$ and R = 0.46, $P < 0.001$, respectively; Fig. 9). In the normal group, CAS was significantly larger in female subjects than male subjects (−0.08 ± 0.04% vs. −0.05 ± 0.03%, $P = 0.003$). In the keratoconus group, CAS was not different between male and female subjects (−0.12 ± 0.06% vs. −0.15 ± 0.11%, $P = 0.707$).

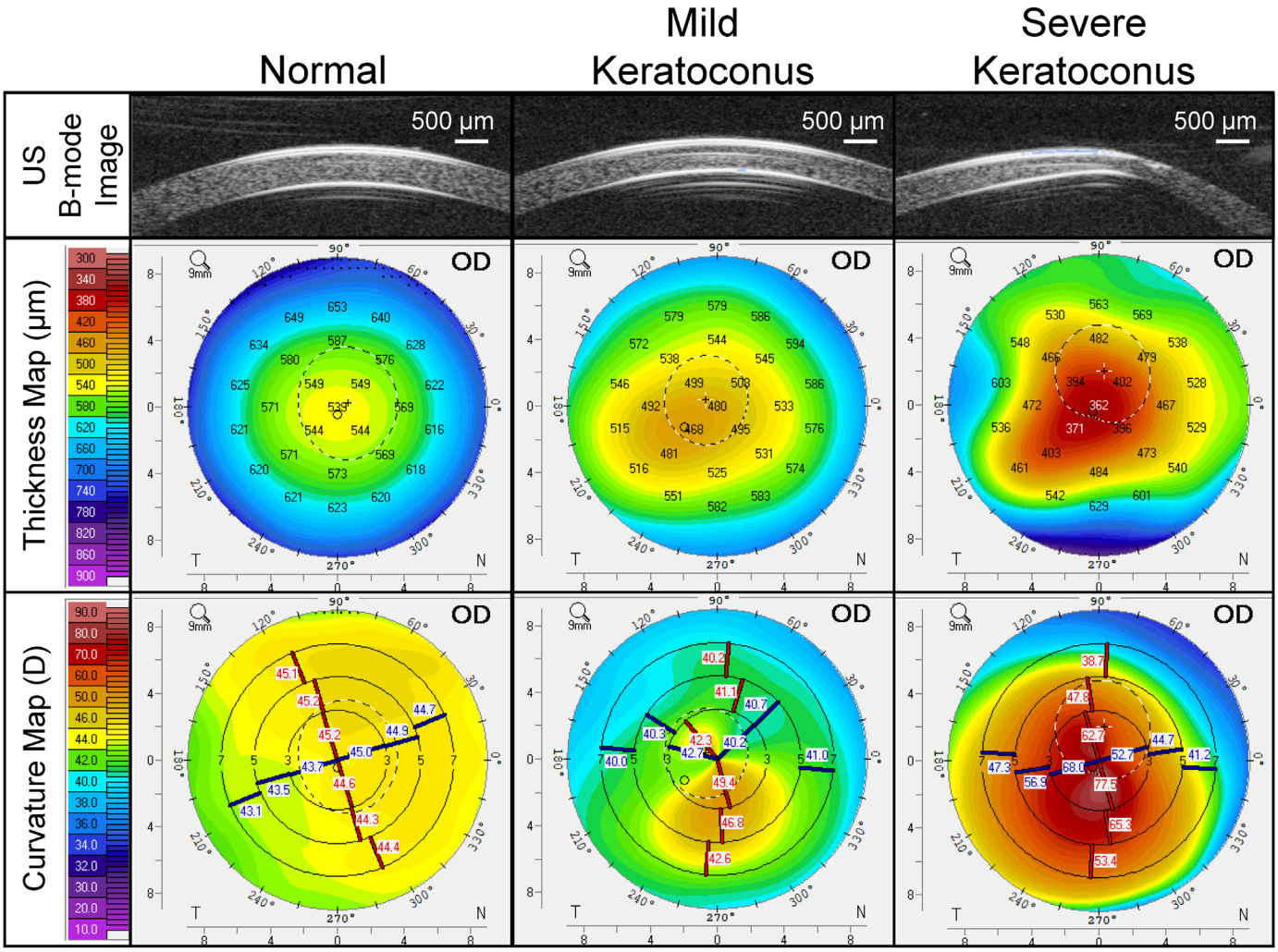

Figure 3. High-frequency ultrasound B-mode images of the central 5.7 mm of the cornea from a normal subject (*left*), grade-2 keratoconus (*middle*), and a patient with grade-4 keratoconus (*right*), along with their corresponding thickness and curvature maps obtained by Pentacam.

Table. Summary Statistics for Age, IOP, OPA, K_{max}, Thinnest Pachymetry, and CAS in 40 Normal Subjects (80 Eyes) and 40 Patients With Keratoconus (63 Eyes)

	Normal		Keratoconus		*P* Values	
	Mean ± SD	Range	Mean ± SD	Range	P*	P**
Age, y	45.8 ± 15.6	[21 to 69]	37.3 ± 12.2	[18 to 74]	**0.0078**	NA
Diastolic IOP, mm Hg	17.4 ± 2.93	[8.8 to 27.0]	15.0 ± 3.7	[5.7 to 23.1]	**<0.001**	NA
OPA, mm Hg	2.57 ± 1.02	[0.87 to 6.03]	2.06 ± 0.72	[0.90 to 4.40]	**0.0011**	**0.029**
K_{max}, D	44.9 ± 1.80	[40.8 to 48.4]	57.2 ± 10.8	[42.7 to 88.5]	**<0.001**	**<0.001**
Thinnest pachymetry, µm	541 ± 36	[468 to 638]	456 ± 57	[294 to 549]	**<0.001**	**<0.001**
CAS, %	−0.06 ± 0.04	[−0.19 to −0.01]	−0.13 ± 0.09	[−0.41 to −0.02]	**<0.001**	**<0.001**

*Without age and IOP as covariates.
**With age and IOP as covariates in the linear mixed model.

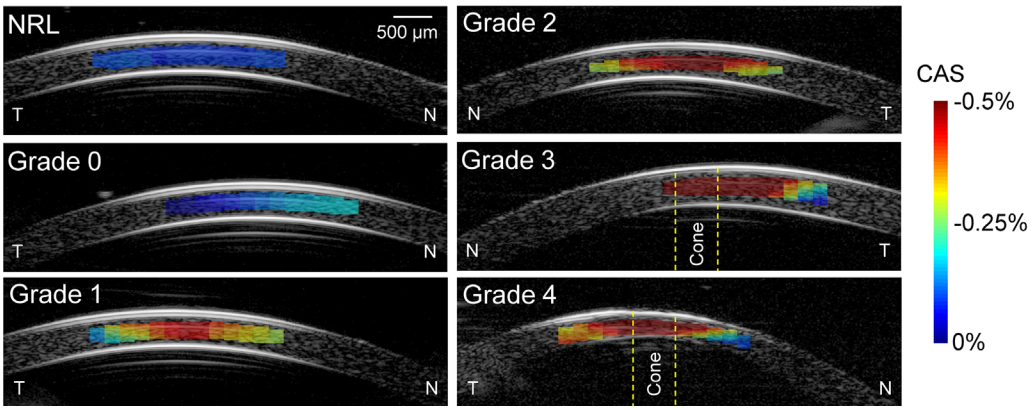

Figure 4. Representative CAS spatial maps for one normal subject (NRL) and a patient from each grade of keratoconus corneas. The cone center in grades 3 and 4 keratoconus is defined as the 500 µm region of stroma centered at the thinnest point of the cornea in the ultrasound B-mode image. CAS in keratoconus corneas was in general higher, especially in the cone center, and more spatially variable.

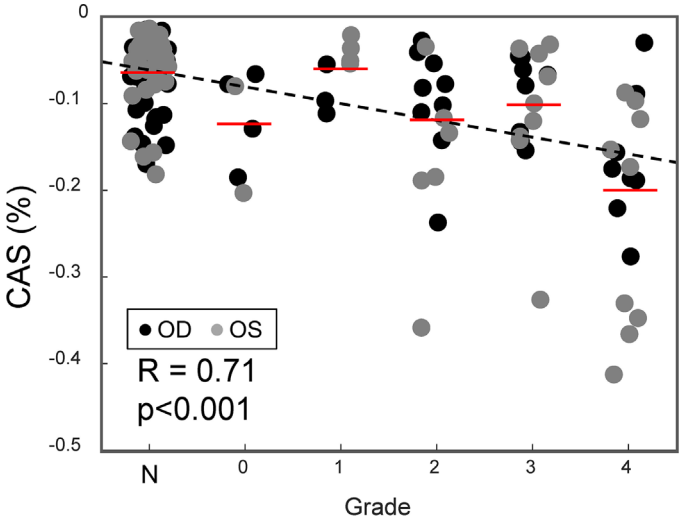

Figure 5. Correlation of CAS to keratoconus grade (N = normal). CAS magnitude increased significantly at higher grade ($P < 0.001$). The *red lines* mark the average value within each grade.

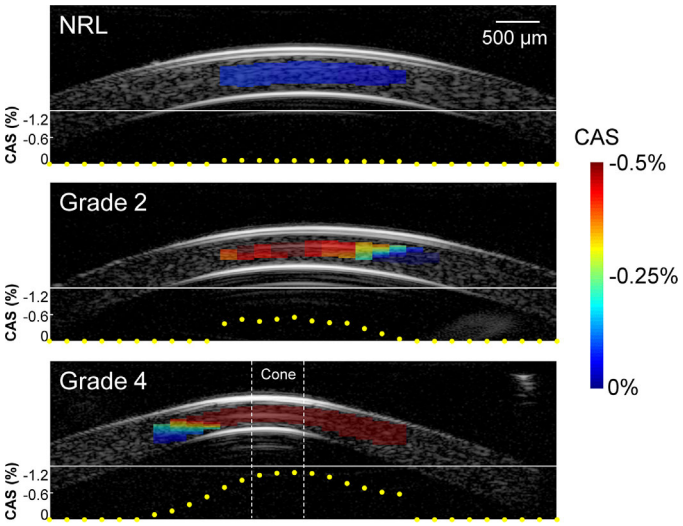

Figure 6. The *yellow dotted lines* show the CAS averaged over the thickness at that location. In the normal (NRL) corneas, CAS was minimal across the width. In the keratoconus corneas, CAS magnitudes were higher, showing a marked increase around the cone.

Discussion

In this study, we developed a working protocol to analyze ultrasound RF data obtained from multiple cardiac cycles to quantify and spatially map the cornea's mechanical response (i.e. CAS) to the ocular pulse. Our main finding is that keratoconus corneas, on average, deformed two times more than the normal corneas in response to IOP fluctuations at each heartbeat. This biomechanical weakening was more pronounced at higher grade keratoconus. We also detected a spatial variation of responses in keratoconus corneas that the cone center had a significantly larger deformation than its surrounding tissue in grades 3 and 4 corneas. In addition, both the cone and the surrounding regions were significantly weaker than the normal cornea.

The CAS is the through-thickness compression of the cornea in response to a change in IOP. The compression associated with the ocular pulse is small in magnitude because of the typically small magnitude of the ocular pulse (on average about 3 mm Hg[25]). A much larger CAS would be expected during larger IOP fluctuations, such as those associated with eye rubbing (80–150 mm Hg[26]). Although the physiological consequences of these IOP-related mechanical strains are unclear, it is reasonable to expect a level of impact on the extracellular matrix (e.g. tear and wear

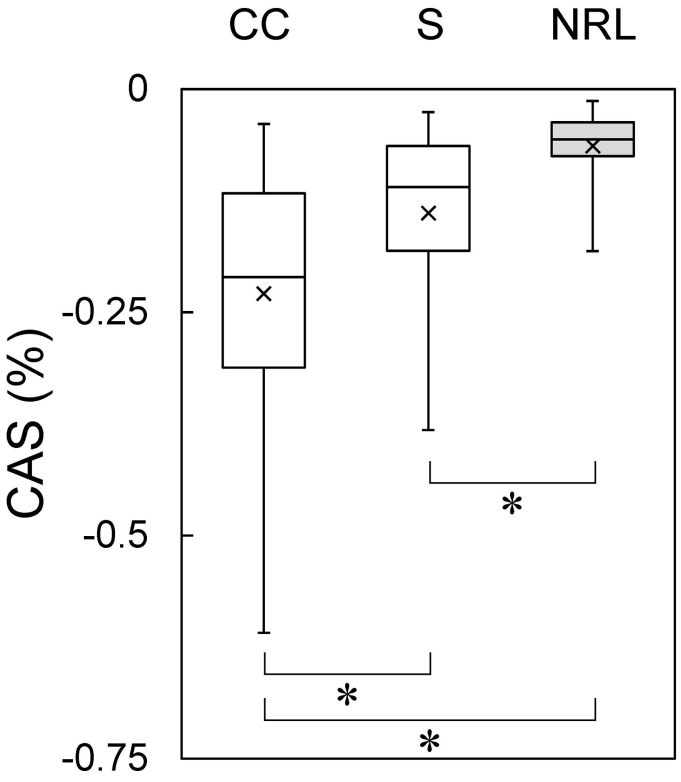

Figure 7. Boxplots showing the significantly larger CAS in the cone center of grades 3 and 4 keratoconus corneas as compared to the surrounding region within the 3-mm ROI. Both the cone center (CC) and its surrounding (S) regions of grades 3 and 4 keratoconus had larger CAS than normal (NRL) corneas. Average values for each group are marked with ×. * Denotes $P < 0.01$.

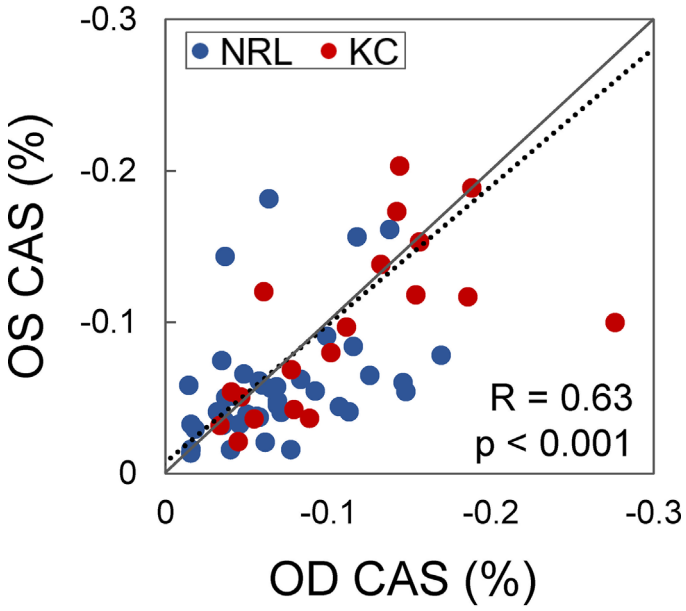

Figure 8. CAS was significantly correlated between the left and the right eyes (R = 0.63, $P < 0.001$) when all measured subjects were combined in the analysis. Significant correlations were also observed in the normal (NRL) and the keratoconus (KC) groups when analyzed separately (normal group: R = 0.38, $P = 0.016$ and keratoconus group: R = 0.61, $P = 0.002$).

over time) and active mechano-stimulation of cellular responses.[27] To our best knowledge, our study is one of the first to quantify the in vivo mechanical deformation of the cornea in response to natural fluctuations of IOP. Most other approaches utilize external mechanical disturbances, such as an air puff,[28] a compression plate,[29] or shear waves.[30] Our OPE method does not require an external mechanical excitation and this brings two advantages. First, the application of an external mechanical load, such as an air puff or a compression plate, alters the instantaneous IOP at the time deformation is measured. Our method does not induce a change in IOP and thus avoids the challenge to account for this change. Second, the application of mechanical disturbances requires additional apparatus and increases the complexity of the overall approach. In terms of ultrasound data acquisition, our method is as straightforward as a clinical B-mode ultrasound. The only difference is that we record a 10-second video of RF data and images of the pulsating cornea for offline analysis. In addition, our method obtains both the loading (i.e. OPA) and the resultant deformation (i.e. CAS). OPA is the pulsating component of the IOP measured by DCT, one of the most reliable devices for measuring OPA[31,32] by averaging over multiple cardiac cycles. Together with the CAS measured by ultrasound, we can define an elastic modulus-like parameter as the ratio of the load (i.e. OPA) and the deformation (i.e. CAS) to characterize corneal mechanical properties in the axial direction.

Our results showed a nearly two times higher deformation in the keratoconic cornea as compared to a normal cornea. In the current study, the age, diastolic IOP, and OPA were statistically different between the normal and the keratoconus subjects. Patients were consecutively recruited at our institute, and we did not control the match of any parameters between groups. Age was higher in the normal group (46 ± 16 years old) than the keratoconus group (37 ± 12 years old). Older age may contribute to tissue stiffening due to glycation-induced crosslinking. The diastolic IOP was also higher in the normal group (17.4 ± 2.93 mm Hg) than the keratoconus group (15.0 ± 3.7 mm Hg). Lower IOP readings in patients with keratoconus were often reported in previous studies,[33,34] but it is believed that the readings were artificially low because the altered corneal properties (thinner and more compliant) in keratoconus are known to cause lower tonometric readings.[35] We used DCT in this study, which was designed to reduce dependence on corneal properties, but it is unclear whether tonomet-

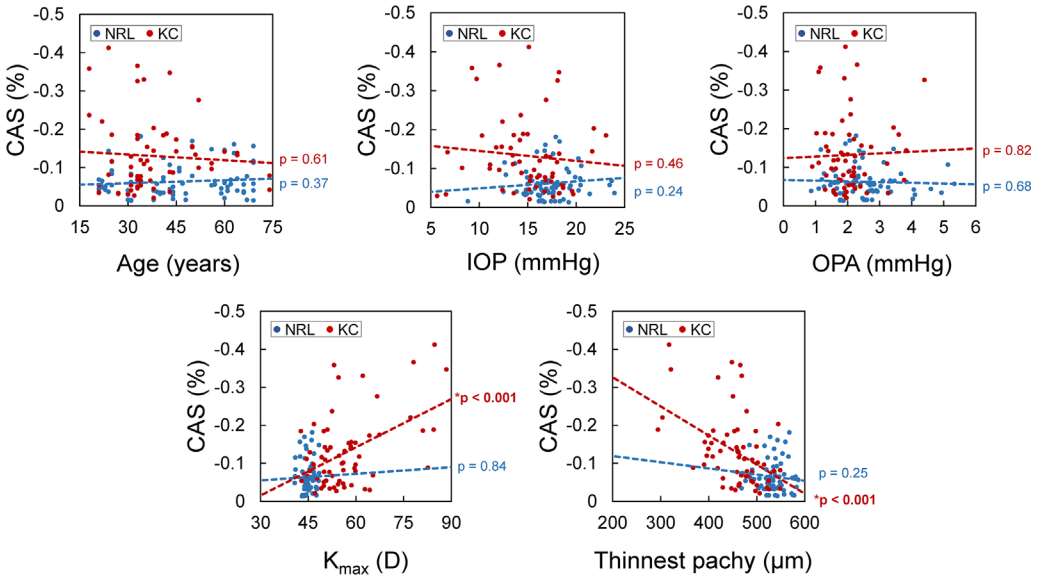

Figure 9. Scatterplots among CAS and age, IOP, OPA, K_{max}, and thinnest pachymetry in the normal (NRL) and the keratoconus (KC) eyes. CAS was not correlated with age, IOP, OPA, K_{max}, or thinnest pachymetry in the normal group (*blue dots*). CAS was correlated with K_{max} and thinnest pachymetry but not age, IOP, or OPA in keratoconus eyes (*red dots*).

ric errors have contributed to the observed difference in IOP. The higher baseline IOP in the normal group may result in a slightly stiffer response due to stress-related stiffening. On the other hand, the normal group had a larger OPA (2.57 ± 1.02 mm Hg) than the keratoconus group (2.06 ± 0.72 mm Hg), which would induce a larger deformation, creating an opposing effect of the older age and larger diastolic IOP. Importantly, CAS remained significantly different between the two groups after considering these covariates (see the Table). In addition, CAS was not correlated with any of these parameters in either the normal or the keratoconus eyes (see Fig. 9), indicating that age, diastolic IOP, and OPA differences were not the main contributors to the CAS difference observed in this study. In contrast, CAS was strongly correlated with K_{max} and thinnest pachymetry in keratoconus, both clinically accepted indicators of keratoconus progression.[36,37] These observations suggest that the CAS difference was more associated with the keratoconus diagnosis and may have potential diagnostic value as indicators of mechanical weakening in keratoconus corneas.

We also observed a trend of increasing CAS at higher grade of keratoconus, consistent with our previous findings of an increasing CAD in higher grades.[18] Grade 4 had the largest CAS, more than 3 times on average than normal, indicating substantial biomechanical compromise as the severest stage. It is noted that although the trend was statistically significant, the current sample size is small and future studies with a larger sample size in each grade are needed to verify this trend. Brillouin imaging showed an increased spatial variance at higher grades.[38] These results together support the "progressive mechanical weakening" hypothesis underlying keratoconus progression.[39,40] We further analyzed the spatial variance of CAS in grades 3 and 4 keratoconus eyes and found that CAS at the cone center (defined as the 500-μm region around the thinnest point in the ultrasound cross-sectional scan of the cornea) was approximately 1.6 times greater than its surrounding tissue in the same eye. Brillouin imaging studies also reported greater mechanical weakening at the cone center.[10,38] The ability to detect regional differences may be useful for planning customized corneal collagen crosslinking (CXL) treatment and monitoring patient outcome. We previously have demonstrated in human donor eyes the feasibility of quantifying CXL-associated stiffening using the OPE technique.[16]

A few limitations of the present study are noted. First, the cone center was defined from ultrasound images based on one B-mode scan through the corneal apex, which is likely not the actual cone center, because the cone is most commonly observed slightly inferotemporal to the apex.[41] Although our current analysis showed a substantial regional biomechanical variation in the keratoconus eye, three-dimensional imaging is needed to fully analyze the extent of spatial variation and to develop sensitive biomechanical markers for keratoconus detection. Second, we only analyzed the axial strains, which characterizes the through-

thickness compression of the cornea. Future studies are needed to develop sensitive and robust methods to characterize the cornea's lateral response (i.e. in-plane stretch), which will add sensitivity to changes in collagen structure. We did not observe an age effect in through-thickness compression in the present study, which may be due to the limited age range, or may be because through-thickness compressive properties are less sensitive to age-associated stiffening. It is noted that the Brillouin frequency shift also showed a minimal age association ($r^2 = 0.08$).[38]

In conclusion, high-frequency ultrasound OPE provides noninvasive, real-time, spatially resolved characterization of the biomechanical responses of the cornea to intrinsic IOP fluctuations. Each measurement takes less than 1 minute to complete. Our results showed the ability of this method to detect and quantify the overall weakening as well as the local variances in keratoconus corneas. High-resolution ultrasound may provide a sensitive tool for quick mapping of corneal biomechanics to aid keratoconus detection and diagnosis.

Acknowledgments

The authors acknowledge the contributions of Kayla Knoll and Daniela Dluzynski for technical assistance in collecting Pentacam and DCT data.

Supported by the (NIH) R01EY025358 and (NIH) R01EY032621.

Disclosure: **S. Kwok**, None; **X. Pan**, None; **M. Pan**, None; **Z. Chen**, None; **M. Ammon**, None; **A. Hendershot**, None; **J. Liu**, None

References

1. Vellara HR, Patel DV. Biomechanical properties of the keratoconic cornea: a review. *Clin Exp Optom*. 2015;98:31–38.
2. Padmanabhan P, Elsheikh A. Keratoconus: a biomechanical perspective. *Curr Eye Res*. 2023;48:121–129.
3. Shetty R, Sathyanarayanamoorthy A, Ramachandra RA, et al. Attenuation of lysyl oxidase and collagen gene expression in keratoconus patient corneal epithelium corresponds to disease severity. *Mol Vis*. 2015;21:12–25.
4. Meek KM, Tuft SJ, Huang Y, et al. Changes in collagen orientation and distribution in keratoconus corneas. *Invest Ophthalmol Vis Sci*. 2005;46:1948–1956.
5. Andreassen TT, Simonsen AH, Oxlund H. Biomechanical properties of keratoconus and normal corneas. *Exp Eye Res*. 1980;31:435–441.
6. Nash IS, Greene PR, Foster CS. Comparison of mechanical properties of keratoconus and normal corneas. *Exp Eye Res*. 1982;35:413–424.
7. Vinciguerra R, Ambrósio R, Elsheikh A, et al. Detection of keratoconus with a new biomechanical index. *J Refract Surg*. 2016;31:803–810.
8. Ambrosio R, Jr., Lopes BT, Faria-Correia F, et al. Integration of Scheimpflug-based corneal tomography and biomechanical assessments for enhancing ectasia detection. *J Refract Surg*. 2017;33:434–443.
9. Lu NJ, Elsheikh A, Rozema JJ, et al. Combining spectral-domain OCT and air-puff tonometry analysis to diagnose keratoconus. *J Refract Surg*. 2022;38:374–380.
10. Randleman JB, Zhang H, Asroui L, Tarib I, Dupps WJ, Jr., Scarcelli G. Subclinical keratoconus detection and characterization using motion-tracking brillouin microscopy. *Ophthalmology*. 2024;131:310–321.
11. Roberts CJ, Dupps WJ. Biomechanics of corneal ectasia and biomechanical treatments. *J Cataract Refract Surg*. 2014;40:991–998.
12. Han Z, Li J, Singh M, et al. Optical coherence elastography assessment of corneal viscoelasticity with a modified Rayleigh-Lamb wave model. *J Mech Behav Biomed Mater*. 2017;66:87–94.
13. De Stefano VS, Ford MR, Seven I, Dupps WJ. Depth-dependent corneal biomechanical properties in normal and keratoconic subjects by optical coherence elastography. *Transl Vis Sci Technol*. 2020;9:4.
14. Scarcelli G, Besner S, Pineda R, Kalout P, Yun SH. In vivo biomechanical mapping of normal and keratoconus corneas. *JAMA Ophthalmol*. 2015;133:180–482.
15. Pavlatos E, Chen H, Clayson K, Pan X, Liu J. Imaging corneal biomechanical responses to ocular pulse using high-frequency ultrasound. *IEEE Trans Med Imaging*. 2018;37:663–670.
16. Clayson K, Pavlatos E, Pan X, Sandwisch T, Ma Y, Liu J. Ocular pulse elastography: Imaging corneal biomechanical responses to simulated ocular pulse using ultrasound. *Transl Vis Sci Technol*. 2020;9:5.
17. Kwok S, Clayson K, Hazen N, et al. Heartbeat-induced corneal axial displacement and strain measured by high frequency ultrasound elastography in human volunteers. *Transl Vis Sci Technol*. 2020;9:33.

18. Kwok S, Pan X, Liu W, Hendershot A, Liu J. High-frequency ultrasound detects biomechanical weakening in keratoconus with lower stiffness at higher grade. *PLoS One*. 2022;17:e0271749.
19. Belin MW, Duncan JK. Keratoconus: the ABCD grading system. *Klin Monatsbl Augenheilkund*. 2016;233:701–707.
20. Tang J, Liu J. Ultrasonic measurement of scleral cross-sectional strains during elevations of intraocular pressure: method validation and initial results in posterior porcine sclera. *J Biomech Eng*. 2012;134:091007.
21. Cruz Perez B, Pavlatos E, Morris HJ, et al. Mapping 3D strains with ultrasound speckle tracking: method validation and initial results in porcine scleral inflation. *Ann Biomed Eng*. 2016;44:2302–2312.
22. Clayson K, Pavlatos E, Ma Y, Liu J. 3D Characterization of corneal deformation using ultrasound speckle tracking. *J Innov Opt Health Sci*. 2017;10:1742005.
23. Ma Y, Pavlatos E, Clayson K, Kwok S, Pan X, Liu J. Three-dimensional inflation response of porcine optic nerve head using high-frequency ultrasound elastography. *J Biomech Eng*. 2020;142:0510131–0510137.
24. Pavlatos E, Chen H, Clayson K, Pan X, Liu J. Imaging corneal biomechanical responses to ocular pulse using high-frequency ultrasound. *IEEE Trans Med Imaging*. 2018;37:663–670.
25. Kaufmann C, Bachmann LM, Robert YC, Thiel MA. Ocular pulse amplitude in healthy subjects as measured by dynamic contour tonometry. *Arch Ophthalmol*. 2006;124:1104–1108.
26. Turner DC, Girkin CA, Downs JC. The magnitude of intraocular pressure elevation associated with eye rubbing. *Ophthalmology*. 2019;126:171–172.
27. Thomasy SM, Leonard BC, Greiner MA, Skeie JM, Raghunathan VK. Squishy matters - corneal mechanobiology in health and disease. *Prog Retin Eye Res*. 2024;99:101234.
28. Dorronsoro C, Pascual D, Perez-Merino P, Kling S, Marcos S. Dynamic OCT measurement of corneal deformation by an air puff in normal and cross-linked corneas. *Biomed Opt Express*. 2012;3:473–487.
29. De Stefano VS, Ford MR, Seven I, Dupps WJ, Jr. Depth-dependent corneal biomechanical properties in normal and keratoconic subjects by optical coherence elastography. *Transl Vis Sci Technol*. 2020;9:4.
30. Lan G, Aglyamov SR, Larin KV, Twa MD. In vivo human corneal shear-wave optical coherence elastography. *Optom Vis Sci*. 2021;98:58–63.
31. Bochmann F, Kaufmann C, Thiel MA. Dynamic contour tonometry versus Goldmann applanation tonometry: challenging the gold standard. *Exp Rev Ophthalmol*. 2010;5:743–749.
32. Kotecha A, White E, Schlottmann PG, Garway-Heath DF. Intraocular pressure measurement precision with the Goldmann applanation, dynamic contour, and ocular response analyzer tonometers. *Ophthalmology*. 2010;117:730–737.
33. Read SA, Collins MJ. Intraocular pressure in keratoconus. *Acta Ophthalmol*. 2011;89:358–364.
34. Firat PG, Orman G, Doganay S, Demirel S. Influence of corneal parameters in keratoconus on IOP readings obtained with different tonometers. *Clin Exp Optom*. 2013;96:233–237.
35. Liu J, Roberts CJ. Influence of corneal biomechanical properties on intraocular pressure measurement: quantitative analysis. *J Cataract Refract Surg*. 2005;31:146–155.
36. Wittig-Silva C, Chan E, Islam FM, Wu T, Whiting M, Snibson GR. A randomized, controlled trial of corneal collagen cross-linking in progressive keratoconus: three-year results. *Ophthalmology*. 2014;121:812–821.
37. Kamiya K, Ishii R, Shimizu K, Igarashi A. Evaluation of corneal elevation, pachymetry and keratometry in keratoconic eyes with respect to the stage of Amsler-Krumeich classification. *Br J Ophthalmol*. 2014;98:459–463.
38. Shao P, Eltony AM, Seiler TG, et al. Spatially-resolved Brillouin spectroscopy reveals biomechanical abnormalities in mild to advanced keratoconus in vivo. *Sci Rep*. 2019;9:7467.
39. Girard MJ, Dupps WJ, Baskaran M, et al. Translating ocular biomechanics into clinical practice: current state and future prospects. *Curr Eye Res*. 2015;40:1–18.
40. Roberts CJ, Mahmoud AM, Bons JP, et al. Introduction of two novel stiffness parameters and interpretation of air puff-induced biomechanical deformation parameters with a dynamic Scheimpflug analyzer. *J Refract Surg*. 2017;33:266–273.
41. Tang M, Shekhar R, Miranda D, Huang D. Characteristics of keratoconus and pellucid marginal degeneration in mean curvature maps. *Am J Ophthalmol*. 2005;140:993–1001.